

Sickle-Shaped Tri-Band MIMO Antenna for 5G and X-Band Applications

Yiwei Tao¹, Han Lin^{1,*}, Ming Yang², Wenyan Nie³, Chenlu Li⁴, and Mingqing Wang¹

¹*School of Electrical and Information Engineering, Anhui University of Science and Technology, Huainan 232001, China*

²*School of Electrical and Communications Engineering, West Anhui University, Lu'an 237012, China*

³*School of Mechanical and Electrical Engineering, Huainan Normal University, Huainan 232001, China*

⁴*School Electrical and Information Engineering, Hefei Normal University, Hefei 230061, China*

ABSTRACT: This paper presents a compact, highly isolated tri-band MIMO antenna for 5G and X-band communication applications. The overall dimensions of the antenna are 43 mm × 30 mm × 1.6 mm. It consists of two monopole radiating units and a metal base with branches and slit slots. The antenna achieves tri-band characteristics by improving the shape of the radiating patch. The isolation of the antenna is enhanced by slotting the floor and loading I- and T-shaped branches to absorb coupling currents. $S_{12} > 15$ dB is achieved in the frequency ranges of 3.3 GHz–4.06 GHz, 4.62 GHz–5.28 GHz, and 8.14 GHz–9.28 GHz. Measurement results show that the measured S -parameters do not change significantly compared with the simulation. It also has a low envelope correlation coefficient and good radiation performance.

1. INTRODUCTION

5G technology has advantages of large broadband, high reliability, and low latency technology, and its application can significantly promote information consumption and the development of artificial intelligence, cloud computing, and other technologies. Satellite communication technology is now also widely used in live television broadcasting, environmental data acquisition, emergency rescue, and other civilian fields. In addition, with the emergence of 5G communication technology and the development of satellite communication technology, there is a growing demand for antennas that can cater to high-capacity data transmission [1]. To accommodate this need, wireless communication systems extensively utilize multiple-input and multiple-output (MIMO) antennas [2]. Because MIMO technology has the characteristics of no increase in spectrum resources and strong resistance to multipath fading, the antenna can make full use of space resources and improve the quality of communication [3]. Recently, researchers have proposed a range of MIMO antennas [4–8]. For example, a novel four-element antenna system has been proposed in [4]. The four elements of this antenna have been placed in opposite positions on either side of the dielectric material for minimal dimensions. The antenna supports the WLAN band ranging from 2.4 GHz to 2.485 GHz and WiMAX band from 3.4 GHz to 3.6 GHz. In [6], a Complementary Split Ring Resonator (CSRR) is designed on the antenna floor, and rectangular patch radiating units are designed on the upper layer to achieve miniaturization of the antenna with improved bandwidth. The antenna generates resonance at 2.4 GHz, 2.9 GHz, and 5.8 GHz, respectively, and can be applied to WLAN communication.

In addition, a dual-port MIMO antenna operating in five frequency bands 2.16 GHz to 2.71 GHz, 3.36 GHz to 4.02 GHz, 5.18 GHz to 5.69 GHz, 7.29 GHz to 8.55 GHz, and 26.02 GHz to 30.39 GHz is proposed in [8].

However, in miniaturized MIMO antenna design, it is necessary to consider how to arrange several antenna units in a limited space and reduce the impact of coupling on antenna performance due to ground current flow and near-field radiation. Many approaches have been proposed for miniaturization techniques. For example, common methods such as loading parasitic patches, bending, slotting, in addition to the use of metamaterials as well as dielectric substrates with high dielectric constants can be used to reduce the antenna size [9–11]. In [12], Shao and Zhang reported a method to achieve size reduction of a conventional rectangular patch antenna by adjusting the separation of coupled microstrip patches. In [13], the overall size of the antenna was reduced by placing modified radiating patches close to each other to reduce unnecessary interaction of the antenna units. In addition, a miniaturized thin hypersurface antenna is proposed in [14]. By introducing a large equivalent parallel plate capacitance through the wall on either side of the square patch, the size of the patch can be reduced by 50%, thereby reducing the overall size of the antenna. The above methods make the antenna more compact but do not solve the problem of MIMO antenna isolation. Many methods have been proposed to enhance isolation, including making the antenna units orthogonal to each other, adding parasitic structures, decoupling network techniques, defective ground structures (DGSs), electromagnetic bandgap (EBG), and other techniques. Qin et al. reported an embedded decoupling structure consisting of two inverted U-shaped branches and two parallel inverted C-shaped branches that can generate additional

* Corresponding author: Han Lin (hanlin@aust.edu.cn).

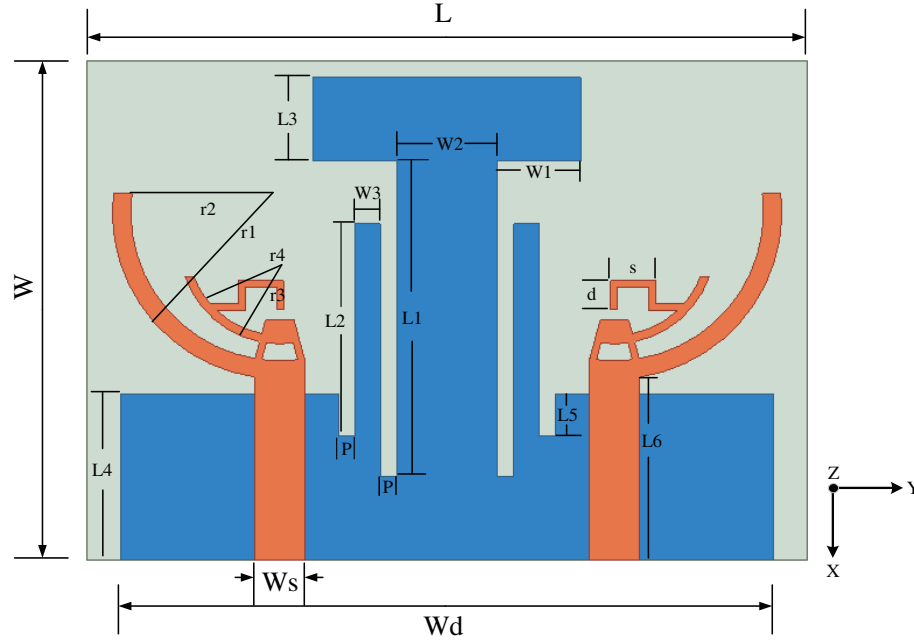


FIGURE 1. Model structure of the antenna.

coupling paths to balance the mutual coupling between antennas [15]. In [16], an L-shaped MIMO antenna was designed to increase the isolation up to 20 dB by combining three methods: T-branch, neutralization line, and defected ground. In [17], the antenna grounding layer was initially inserted with multiple slots based on a defective grounding structure, resulting in an antenna isolation of 23.5 dB. The dual-port MIMO antenna is then placed on the hypersurface's upper layer, producing a higher isolation of 51 dB.

In summary, this paper presents a novel dual-port tri-band MIMO antenna structure that contains two symmetric sickle-shaped radiating units, an improved defective ground structure, and a T-neutralization line to improve isolation by efficiently absorbing currents and reducing the coupling between the radiating units. Multiple frequencies are generated using multiple circular branching structures of the radiating unit and an improved grounding structure to broaden the operating bandwidth by improving the impedance matching at each frequency. The antenna's three operating bandwidths of 3.3 GHz–4.06 GHz, 4.62 GHz–5.28 GHz, and 8.14 GHz–9.28 GHz cover China's 5G communication bands of 3.3 GHz–3.6 GHz and 4.8 GHz–5.0 GHz, respectively, as well as the X-band used for satellite communications. In addition, antenna isolation is greater than 15 dB in all three bands. Also, this sickle-type MIMO antenna has good diversity and radiation performance. The remaining paper is organized as follows. Section 2 discusses the design process of the antenna, parametric simulation studies, and the analysis of surface currents. Section 3 discusses the experimental results obtained from the fabricated prototype. Finally, Section 4 concludes this paper.

2. ANTENNA DESIGN

2.1. Antenna Geometry

The antenna geometry can be seen in Figure 1. The proposed antenna structure consists of two identical and symmetrical sickle-shaped radiating units fed through a microstrip line. Each unit consists of a circular branch with 90 degrees of arc, a circular branch with 70 degrees of arc, an inverted U-shaped branch, and a trapezoidal patch. In addition, the back portion of the antenna is metal ground, where a T-shaped branch is directly connected to the ground; two I-shaped branches flank the T-shaped branch; and four rectangular slots are added to the ground. The antenna is printed on a 43 mm × 30 mm × 1.6 mm FR4 dielectric substrate with a 4.4 relative permittivity and 0.02 loss tangent. Table 1 shows the specific dimensional details of the sickle-shaped MIMO antenna.

The longer arc branch generates the antenna's 3.8 GHz frequency resonant mode. In addition, the 4.8 GHz frequency resonant modes are activated by loading shorter curved branches and inverted U-shaped branches. These two resonance points can be controlled separately to some extent, allowing for greater design flexibility. In addition, the antenna's high-frequency resonant mode is generated by the combined action of the end of the inverted U-shaped branch, the loaded rectangular patch radiating unit, and the floor.

2.2. Design Analysis of Antenna Structures

2.2.1. Evolution of The Antenna Structure

Figure 2 shows the evolution of the antenna structure. The evolution of the antenna structure is shown in Figure 2. Referring

TABLE 1. Optimized dimensional parameters of the antenna.

Parameters	L	W	Wd	W_s	$W1$	$W2$	$W3$	$L1$
dimensions (mm)	43	30	39	3	5	6	1.5	19
Parameters	$L2$	$L3$	$L4$	$L5$	$L6$	$r1$	$r2$	$r3$
dimensions (mm)	12.7	5	10	2.5	11	10	8.9	6
Parameters	$r4$	d	s	P				
dimensions (mm)	5.5	1.75	2.7	1				

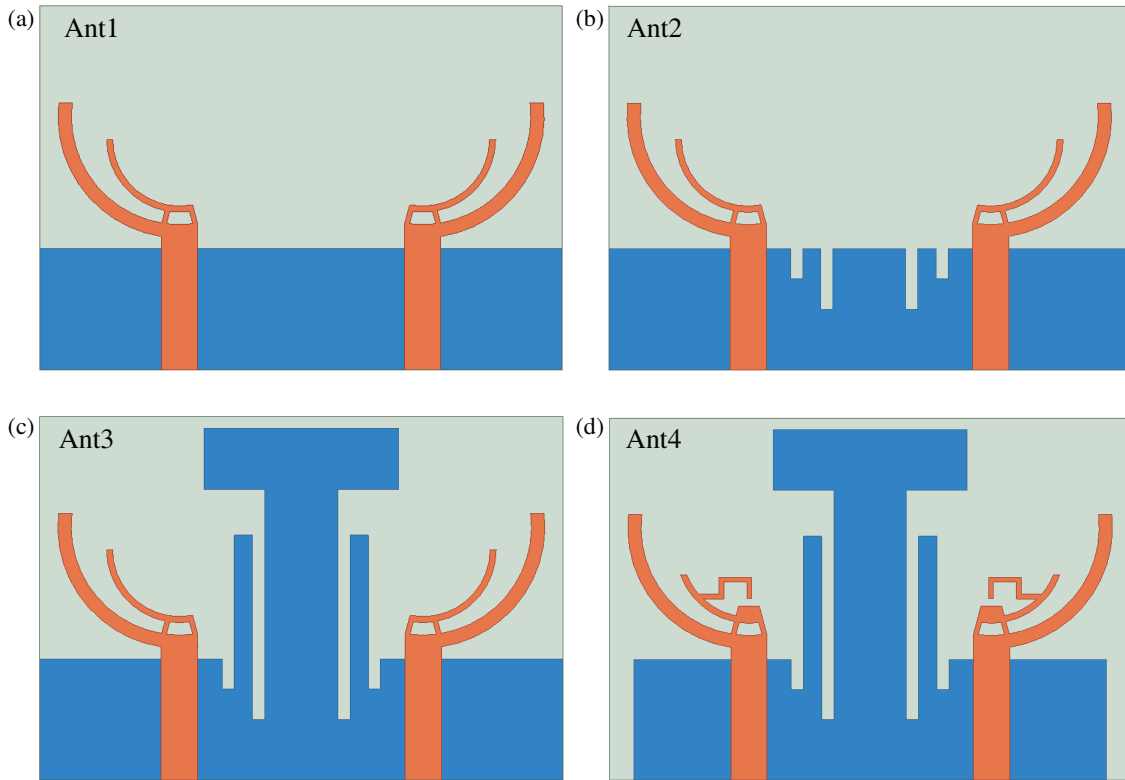


FIGURE 2. Evolution of antenna structure: (a) Ant1, (b) Ant2, (c) Ant3, and (d) Ant4.

to Figure 2(a), an arc branch with an arc of 90 degrees and an arc branch with an arc of 100 degrees are designed to realize the 5G dual bands. The lengths and resonant frequencies of the two arc branches are calculated through the following equations, respectively [18]:

$$L_{S1} = \frac{1}{2} \times r1 \times \pi \quad (1)$$

$$L_{S2} = \frac{5}{9} \times r3 \times \pi \quad (2)$$

$$f_s = \frac{c}{4L_S \sqrt{\epsilon_{reff}}} \quad (3)$$

where ϵ_{reff} is half of the FR4 dielectric constant; L_{S1} is the effective length of the arc branch with an arc of 90 degrees; L_{S2} is the effective length of the arc branch with an arc of 100 degrees; f_s is the resonance frequency; c is the propagation speed of the

electromagnetic wave; and L_s denotes L_{S1} or L_{S2} . The designed resonance frequencies are calculated to be 3.4 GHz and 4.9 GHz. both are at the center frequency position of the 5G dual bands. However, Figure 3(a) shows that both resonances at the lower frequencies are shifted to the right compared to theoretical design. In addition, due to the interaction between the floor and radiating unit, a resonance point in the X-band is created. In addition, the isolation of the antenna is relatively poor, approaching -10 dB for all three bands.

As shown in Figure 2(b), a slit-slot structure is designed on the floor to improve the isolation of the antenna. The flow direction of the floor current is changed to weaken the coupling between the antennas. Figures 3(a) and (b) show that the antenna's resonance point remains unchanged, but the isolation of the high-frequency portion of the antenna drops to -15 dB.

As shown in Figure 2(c), to further enhance the antenna isolation, additional T-branches and I-branches are added to create extra coupling paths on the back floor. The antenna unit on

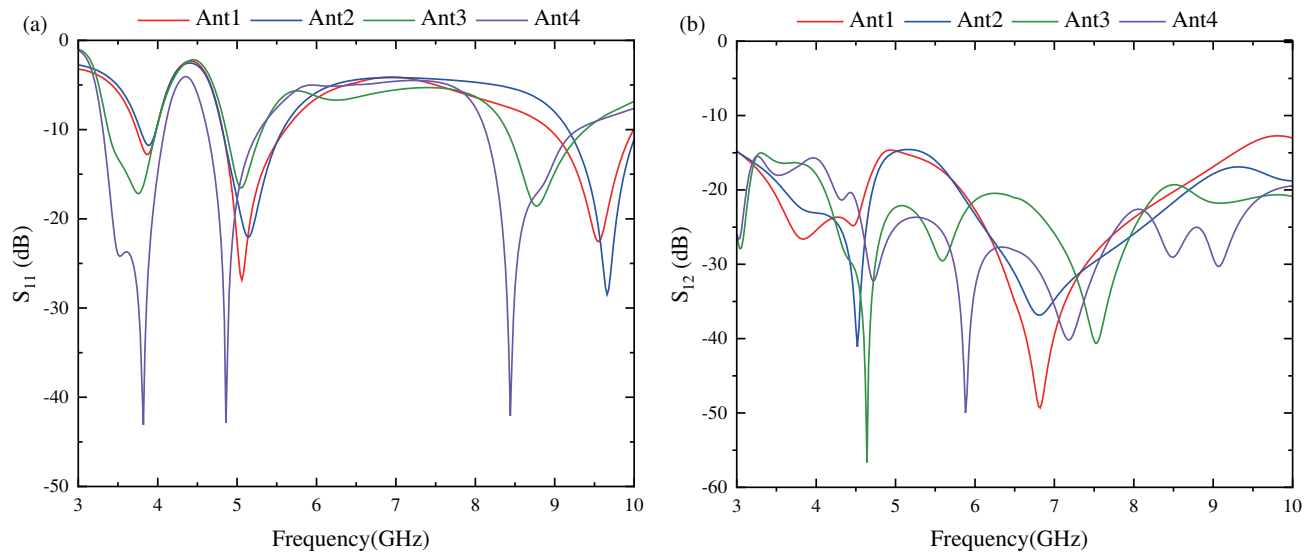


FIGURE 3. S -parameter simulation of 4 antenna structures: (a) S_{11} and (b) S_{12} .

port 1 is coupled to the antenna units on the T-branch, I-branch, and port 2. It is through this interaction that improved antenna isolation is achieved. As a result, S_{12} drops below -20 dB at around 4.9 GHz, and the isolation is close to -20 dB in the high-frequency part. In addition, as seen in Figure 3(a), the increase of the T-branches as well as the I-branches shifts the high-frequency resonance point to the left.

This is the final structure of the antenna as shown in Figure 2(d). To make the antenna work closer to the 5G dual bands as well as the X-band, a rectangular metal ground was cut away from each side of the floor; the thinner curved branches of the radiating unit were shortened; and an inverted U-shaped branch and a trapezoidal patch were attached to it. Referring to Figures 3(a) and (b), the two low-frequency resonances of the antenna are shifted to 3.8 GHz and 4.8 GHz; the high-frequency resonance is shifted to the left; and the return loss of all bands reaches 40 dB due to the changes in the shape of the floors and radiating units, resulting in a better impedance matching. The antenna's final three band ranges are 3.3 GHz to 4.06 GHz, 4.62 GHz to 5.28 GHz, and 8.14 GHz to 9.28 GHz, providing full coverage of the 5G dual bands as well as some of the X-band. In addition, the antenna's high-frequency operating band isolation is reduced to below -20 dB, and the isolation of the 5G band is below -15 dB.

2.2.2. Antenna Parameter Optimization

In order to optimize the capability of the designed dual-port tri-band antenna, some key dimensions of the antenna are optimized using HFSS simulation software. The optimization process follows the principle of optimizing one dimension while keeping the other dimensions unchanged, and the optimization results are shown in Figure 4. From Figures 4(a), (b), (c), it can be seen that the parameters r_2 , r_4 , and Wd mainly affect the resonant frequency of the antenna as well as the impedance matching of the antenna. As shown in Figure 4(a), there is no

significant change in the individual resonant frequencies of the antenna as r_2 is increased up to 8.9 mm, whereas when r_2 is equal to 9.1 mm, there is an impedance mismatch in the middle band of the antenna, and the low-frequency resonance point is shifted to the left. In addition, when r_2 is equal to 8.9 mm, the antenna shows good return loss at each resonant frequency. As shown in Figure 4(b), the resonant frequencies of the middle and high frequencies are shifted to the left as r_4 increases, and the operating bandwidth still covers the 5G and X bands. When r_4 is 5.5 mm, the antenna has the best return loss performance at the three resonant frequencies. As shown in Figure 4(c), there is no significant change in the three frequency points of the antenna as Wd is reduced to 39 mm. When Wd is 38 mm, the low-frequency resonance point is shifted to the left. In addition, when Wd is 39 mm, the return loss at the resonant frequency shows the best performance. In summary, the optimum results are 8.9 mm for r_2 , 5.5 mm for r_4 , and 39 mm for Wd , which can get the optimum impedance matching and frequency coverage from 3.3 GHz to 4.06 GHz, 4.62 GHz to 5.28 GHz, and 8.14 GHz to 9.28 GHz.

2.2.3. Discussion of Antenna Surface Current

Figure 5 shows the current distribution in the high-frequency part of Ant1 and Ant2 and further analyzes the effect of variation in the metallic ground on the antenna coupling. Referring to Figure 5(a), a part of the current is coupled to the right antenna under the excitation of the left port 1. In Figure 5(b), the introduction of the defective ground structure reduces this coupling effect.

Figure 6 shows the low-frequency current distributions for Ant2, Ant3, and Ant4, and further analyzes the effect of the variation of the backplane cross-section on the antenna isolation as well as the effect of the improved radiating unit on the antenna radiation performance. From Figure 6(a), the right antenna has a high current coupling under the excitation of port

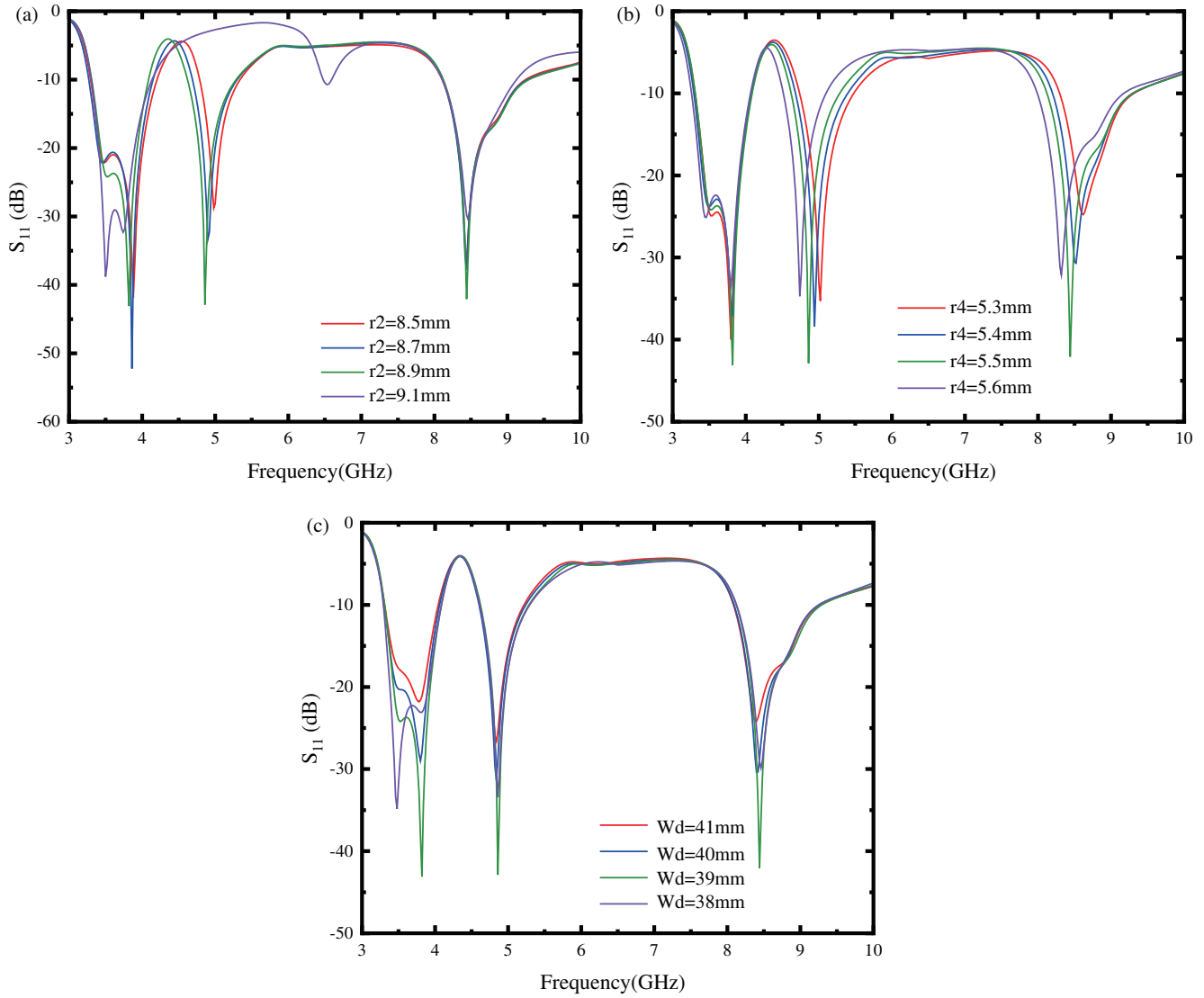


FIGURE 4. Effect of different size variations on antenna S_{11} : (a) r_2 , (b) r_4 , and (c) W_d .

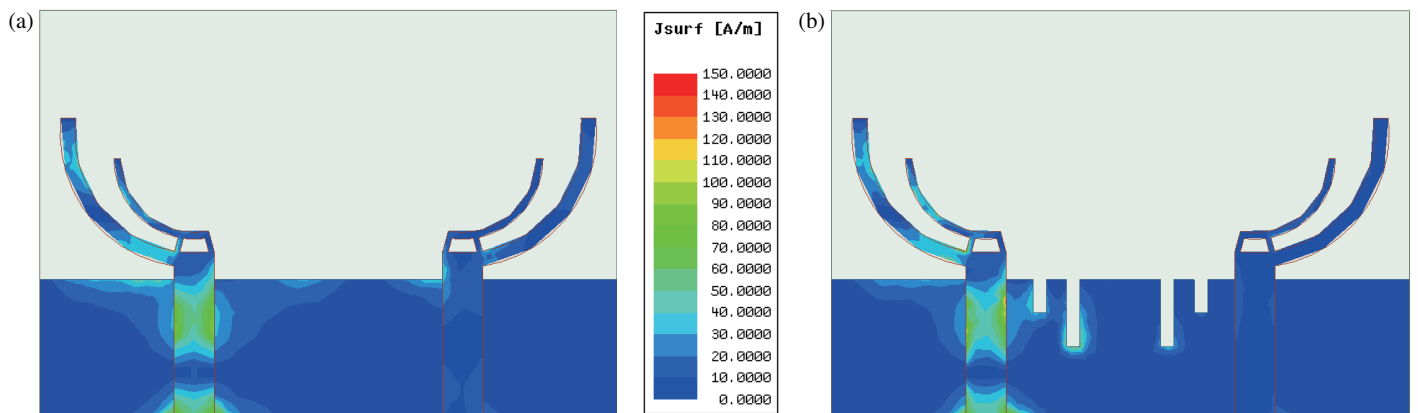


FIGURE 5. Ant1 and Ant2 surface current distribution.

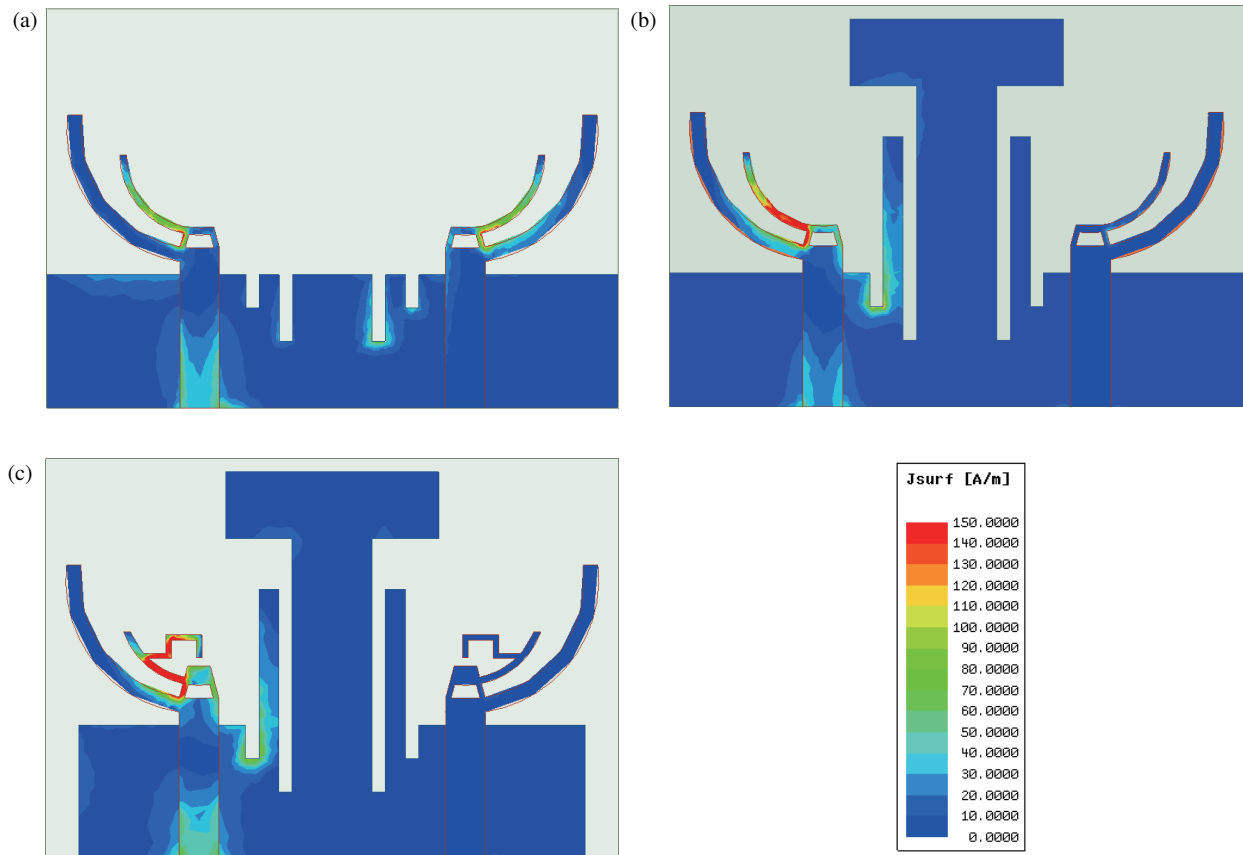


FIGURE 6. Ant2, Ant3 and Ant4 surface current distribution.

1. Moreover, in Figure 6(b), trace currents are observed in the right antenna due to the introduction of I-branches as well as T-branches, which reduces this coupling effect. Finally referring to Figure 6(c), the change in the floor length as well as the improvement in the radiating cell results in higher current strength of the metal patch, better impedance matching of the antenna, and improved radiating performance.

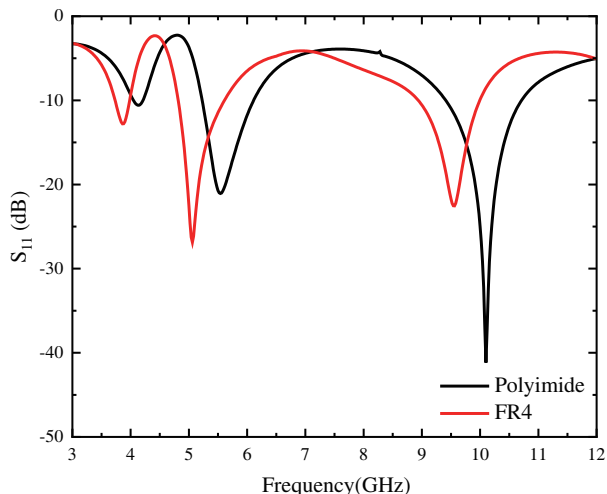


FIGURE 7. Comparison of S_{11} -parameters using different substrates.

2.3. Comparison with Flexible Antennas

For a reasonable comparison, we here replace the FR4 substrate with a polyimide flexible material based on the Ant1 structure in Figure 2(a). In addition, the length of the curved branch is lengthened according to Equations (1) and (3) because of the change in the substrate dielectric constant.

As shown in Figure 7, the number of resonance points of the antenna does not change, and the resonance frequencies are all shifted to the right to varying degrees. In addition, better impedance matching is obtained for the high-frequency resonance points. The structure of the antenna is relatively stable and has not changed dramatically due to the replacement of the substrate material. Moreover, it also shows that the antenna can be optimized with an appropriate structure, which makes it possible to produce the desired 5G band and X-band even with a flexible substrate.

3. RESULTS AND DISCUSSION

3.1. S-Parameters

An Agilent N5235A vector network analyzer is used to measure the S -parameters of the antenna. Figure 8 shows the measurement environment of the antenna microwave darkroom and the prototype that was produced. From Figure 9(a), S_{11} measurements of the antenna closely match the simulation results. In the

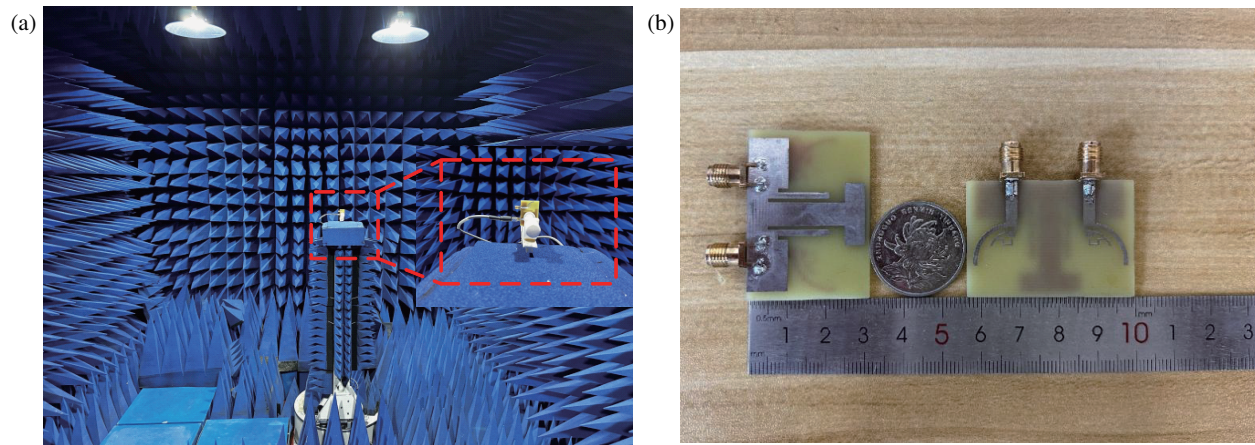


FIGURE 8. The proposed antenna. (a) Antenna microwave darkroom measurement environment and (b) Antenna object.

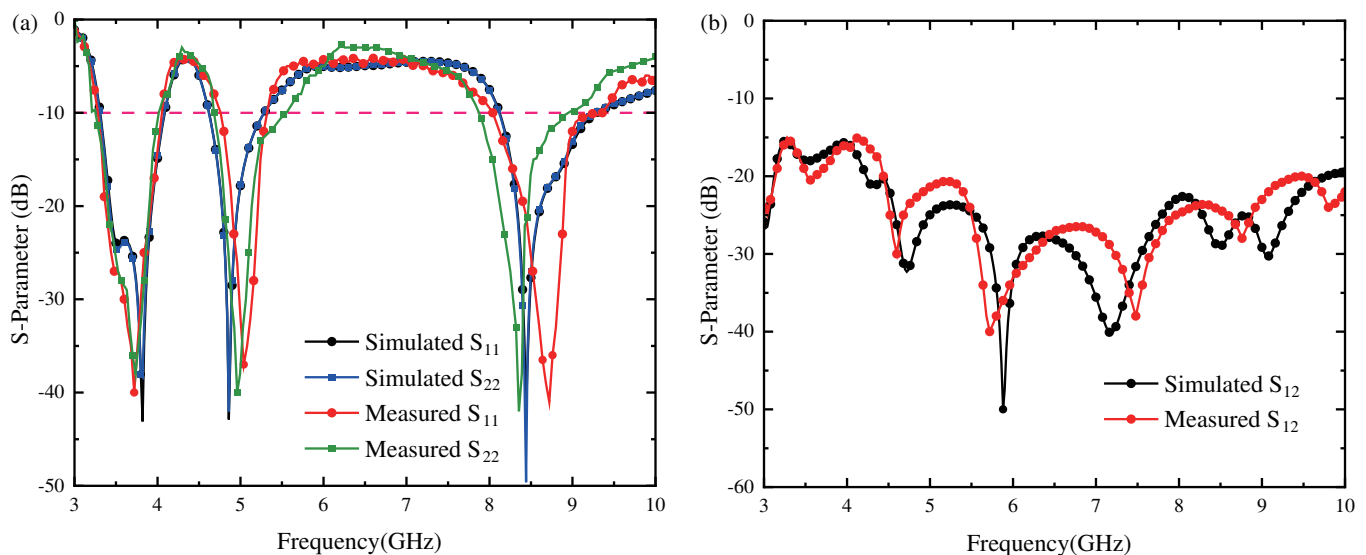


FIGURE 9. MIMO antenna simulated and measured S -parameters: (a) S_{11} and (b) S_{12} .

measured frequencies, the low frequencies are slightly shifted to the left, and the middle and high frequencies are slightly shifted to the right. The measured S_{11} band includes 3 GHz to 4.04 GHz, 4.76 GHz to 5.32 GHz, and 8.04 GHz to 9.36 GHz, and the measured S_{22} band consists of 3.26 GHz to 4.01 GHz, 4.68 GHz to 5.5 GHz, and 7.8 GHz to 8.9 GHz. Furthermore, SMA connector and line losses, as well as test conditions, can lead to faults. Referring to the S_{12} parameter curve shown in Figure 9(b), the antenna isolation is greater than 15 dB, thus achieving higher isolation between the two ports in the MIMO antenna.

3.2. Radiation Capacity

Figure 10 depicts the E -plane and H -plane gain radiation patterns of the antenna at 3.8 GHz, 4.8 GHz, and 8.4 GHz. The E -side at both 3.8 GHz and 4.8 GHz exhibits a dumbbell-like shape, and the H -side exhibits a love heart shape rotated 90 de-

grees counterclockwise. The maximum radiation direction of the E -plane ranges from 300 degrees to 30 degrees and from 150 degrees to 210 degrees, while the maximum radiation direction of the H -plane ranges from 150 degrees to 30 degrees. At 8.4 GHz, the E -plane and H -plane are distorted and show a petal shape. Among them, the E -plane radiates more strongly between 330 degrees and 0 degrees, and the H -plane shows better directional radiation with more prominent radiation gain at 270 degrees. Generally, the antenna shows good radiation capability and good gain at all three frequency points. The designed antenna has good performance in receiving signals from different directions, thus achieving excellent radiation capability.

Figure 11 shows the antenna's gain variation and radiation efficiency results in each frequency band. The antenna's gain varies from around 2.4 dBi to 7.5 dBi. Furthermore, the antenna features a high radiation efficiency of over 77% across the frequency range.

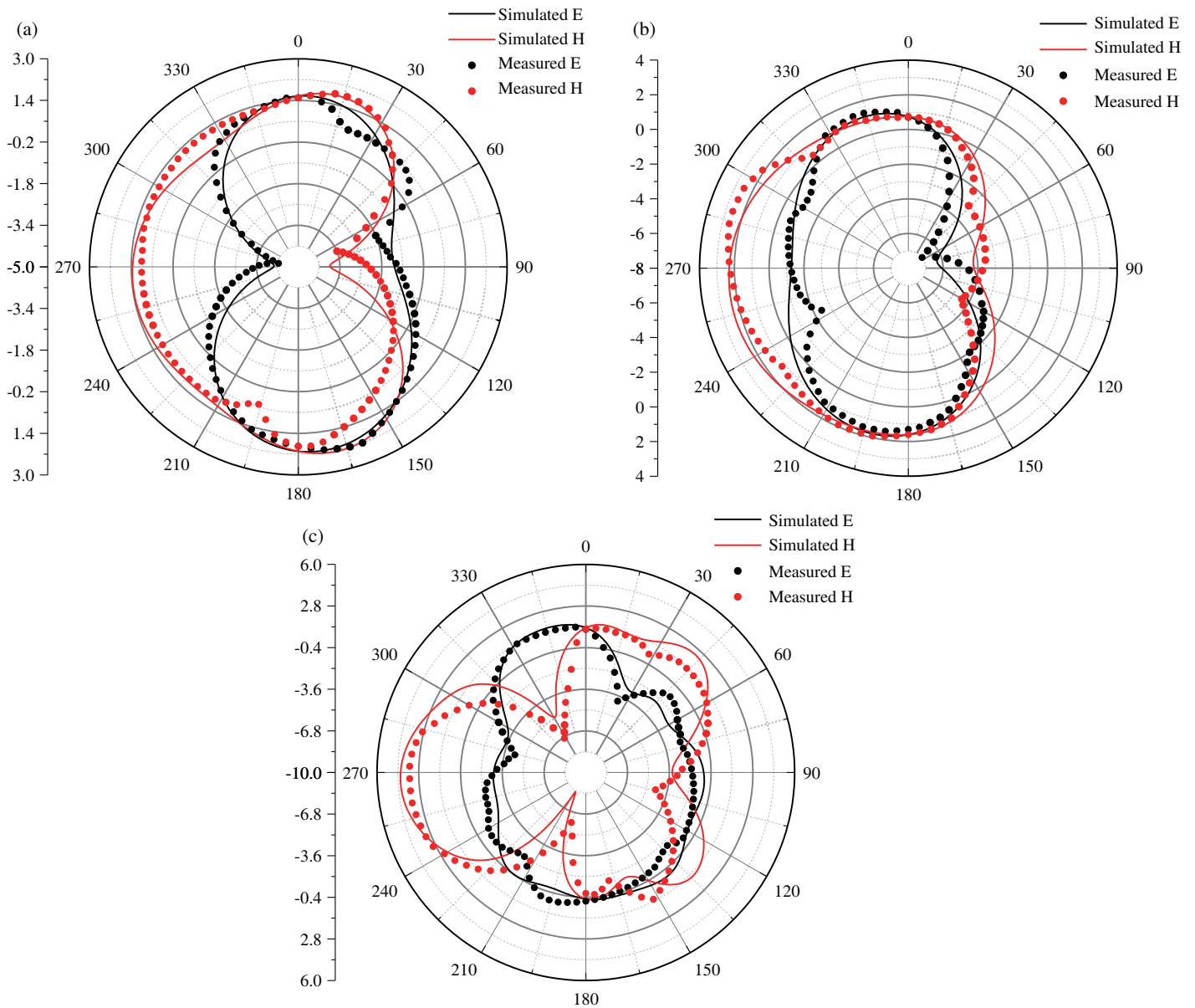


FIGURE 10. The radiation patterns were simulated and measured at three different frequencies: (a) 3.8 GHz, (b) 4.8 GHz, and (c) 8.4 GHz.

3.3. Diversity Performance of MIMO Antenna

3.3.1. ECC

To characterize the correlation between the received signal amplitudes between different antenna units, we use envelope correlation coefficient (ECC) to measure the antenna diversity performance and coupling performance. After many tests, it was found that the antenna can work better when the ECC is lower than 0.5. For the antenna designed in this paper, the following formula can calculate the ECC:

$$\rho_{ij} = \frac{|\iint_{4\pi} \bar{F}_i(\theta, \phi) \cdot \bar{F}_j^*(\theta, \phi) d\Omega|^2}{\iint_{4\pi} |\bar{F}_i(\theta, \phi)|^2 d\Omega \cdot \iint_{4\pi} |\bar{F}_j(\theta, \phi)|^2 d\Omega} \quad (4)$$

Moreover, Figure 12 shows the ECC value of the antenna to be below 0.01 in the frequency band, meeting the standard.

3.3.2. TARC

To ensure that the designed MIMO antenna system has low reflection loss and good phase stability, we introduce the measure of Total Effective Reflection Coefficient (TARC). Typically, TARC should be less than -10 dB to ensure reliable signal transmission. The following equation calculates the TARC of the antenna:

$$\text{TARC} = -\sqrt{\frac{(S_{11} + S_{12})^2 + (S_{21} + S_{22})^2}{2}} \quad (5)$$

As illustrated in Figure 13, the TARC value of the antenna is below 20 dB within the studied range, indicating a low coupling effect. The lower TARC ensures the independence of the various channels on the transmitter and receiver sides of the MIMO system. The multipath effect can be effectively exploited to improve the system's capacity.

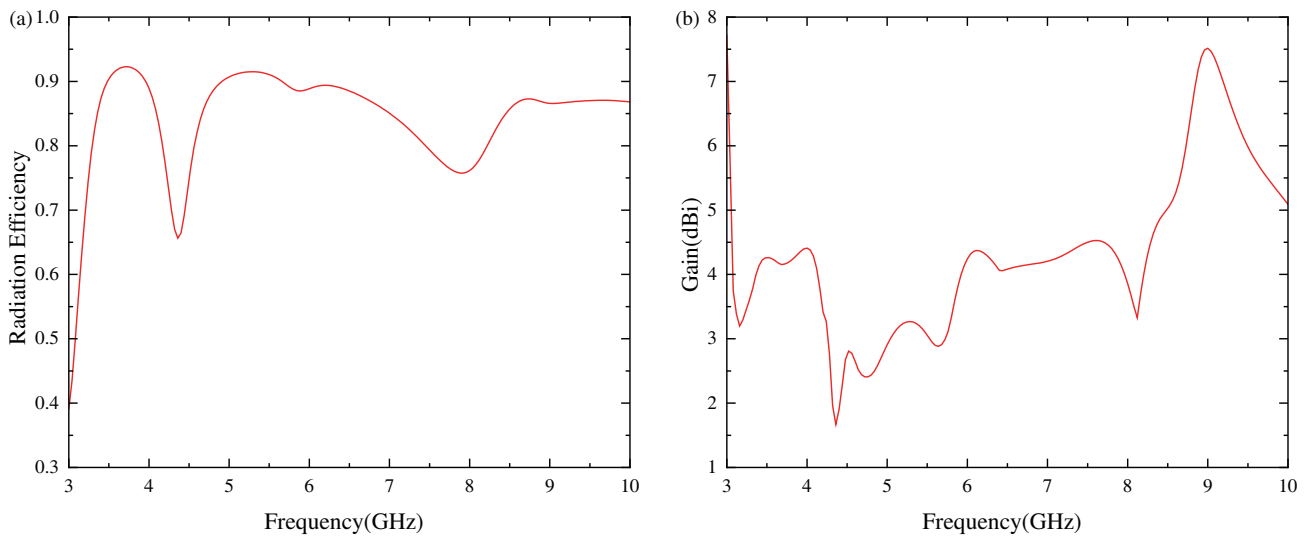


FIGURE 11. The proposed antenna: (a) radiation efficiency and (b) gain.

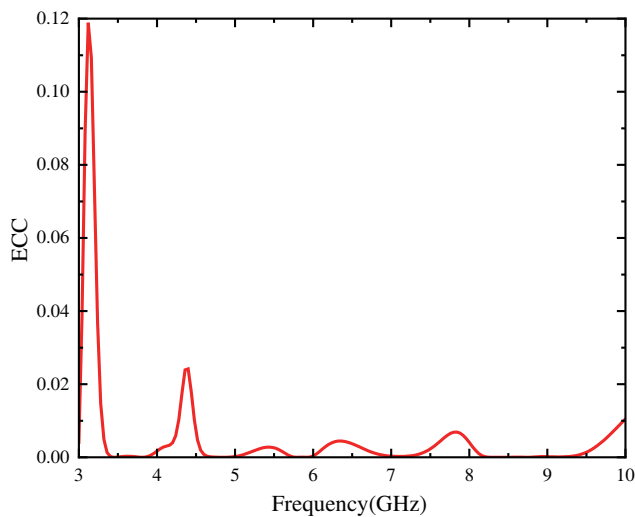


FIGURE 12. ECC of the antenna.

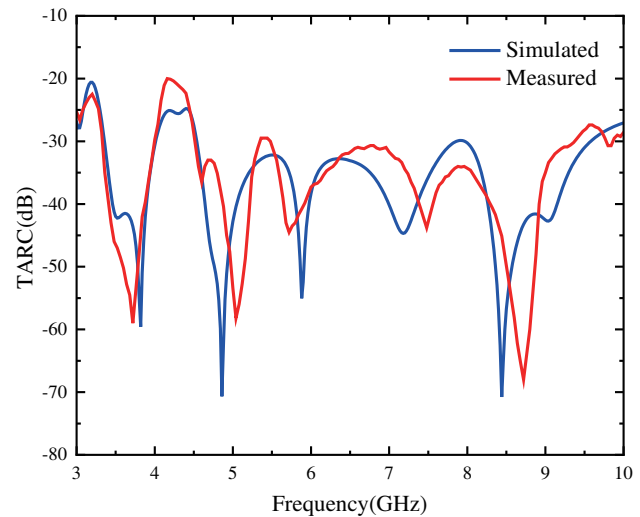


FIGURE 13. Proposed TARC for two-port antennas.

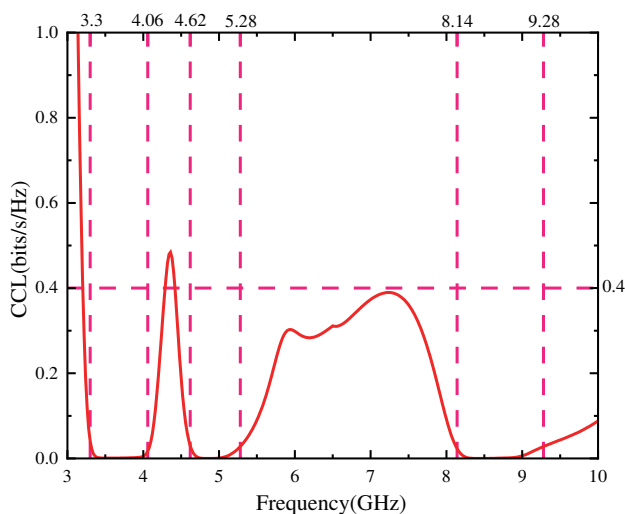


FIGURE 14. CCL of the antenna.

3.3.3. CCL (Channel Capacity Loss)

In MIMO antennas, CCL is also an important metric for determining the diversity performance of the antenna. The CCL in a MIMO system must be less than 0.4 bits/s/Hz to be considered acceptable. As shown in Figure 14, the CCL is significantly lower than 0.4 bits/s/Hz in the operating band achieved by the antenna, which is within the acceptable range.

3.4. Comparative Study

A comprehensive comparison of the proposed antenna with several MIMO antennas reported in Table 2 in terms of isolation, antenna radiation efficiency, etc. is presented below. The proposed antenna has higher isolation, smaller size, and better radiation performance than [2], better radiation performance along with diversity performance than [16], more available frequency bands than [19–26], a smaller size than [20, 23, 24], and higher isolation and radiation performance than [22, 26].

TABLE 2. Proposed MIMO antenna performance comparison with others.

Ref.	Size (mm × mm × mm)	Operating frequency (GHz)	Isolation	Radiation Efficiency (%)	ECC
[2]	56.4 × 36.6 × 1.524	3.37–3.6, 4.76–5.15, 6.22–7.27	> 13	> 50	< 0.2
[16]	50 × 25 × 0.8	4.4–4.9, 5.4–6.1, 7.0–7.4	> 20	> 70	< 0.04
[19]	32 × 32 × 1.59	2.36–2.59, 3.17–3.77	> 15	> 76	< 0.02
[20]	64 × 64 × 1.6	3.0–4.4, 5.0–6.6	> 18	> 92	< 0.03
[21]	34 × 25 × 1.6	3.3–6.3	> 20	\	< 0.02
[22]	13.3 × 4 × 1	3.35–3.67	> 10	> 43	\
[23]	50 × 50 × 1.59	2.25–3.15, 4.80–5.95	> 15	> 77	< 0.01
[24]	48 × 48 × 1.6	2.25–2.41, 4.7–6.25	> 18	\	< 0.2
[25]	22 × 13 × 0.254	24.6–42.1 50.1–52.5	> 66	> 98.7	0.002, 0.001
[26]	50 × 50 × 1.6	5.47–7.08 7.28–8.54	> 13	\	< 0.1
This work	43 × 30 × 1.6	3.3–4.06, 4.62–5.28, 8.14–9.28	> 15	> 77	< 0.01

In conclusion, the proposed antenna has better overall performance and can be applied to different mobile communication devices. The performance comparison of the proposed MIMO antenna with other works is shown in Table 2.

4. CONCLUSION

This paper describes the design of a simple and compact tri-band MIMO antenna with high isolation. The antenna is suitable for 5G and X-band applications. The antenna consists of two symmetric sickle-shaped monopole radiating units. Each unit consists of a circular branch with 90 degrees of arc, a circular branch with 70 degrees of arc, an inverted U-shaped branch, and a trapezoidal patch. The isolation of >15 dB in the frequency ranges of 3.3 GHz–4.06 GHz, 4.62 GHz–5.28 GHz, and 8.14 GHz–9.28 GHz is achieved by loading the branches and floor gap. Finally, this dual-port MIMO antenna has a simple design, easy fabrication, low cost, high radiation efficiency as well as low ECC for 5G and X-band communications.

ACKNOWLEDGEMENT

This work was supported in part the Natural Science Research Project of Anhui Educational Committee under No. 2022AH051583, No. 2022AH052138 and No. 2023AH052650, in part by the Anhui Province Graduate Academic Innovation Project under grant No. 2023xscx074, in part by the Graduate Innovation Fund of Anhui University of Science and Technology under grant No. 2024cx2063.

REFERENCES

- [1] Chung, M.-A., C.-C. Hsu, M.-C. Lee, and C.-W. Lin, “Enhancing multi-band MIMO antenna stability for various electronic applications with human-body interaction consideration,” *IEEE Access*, Vol. 11, 129 376–129 398, 2023.
- [2] Wang, Z., W. Ren, W. Nie, W. Mu, and C. Li, “Design of three-band two-port MIMO antenna for 5G and future 6G applications based on fence-shaped decoupling structure,” *Progress In Electromagnetics Research C*, Vol. 134, 249–261, 2023.
- [3] Ullah, R., S. Ullah, F. Faisal, R. Ullah, I. B. Mabrouk, M. J. A. Hasan, and B. Kamal, “A novel multi-band and multi-generation (2G, 3G, 4G, and 5G) 9-elements MIMO antenna system for 5G smartphone applications,” *Wireless Networks*, Vol. 27, No. 7, 4825–4837, 2021.
- [4] Ali, W. A. E., M. I. Ashraf, and M. A. Salamin, “A dual-mode double-sided 4 × 4 MIMO slot antenna with distinct isolation for WLAN/WiMAX applications,” *Microsystem Technologies*, Vol. 27, No. 3, 967–983, 2021.
- [5] Aliqab, K., A. Armghan, and M. Alsharari, “A versatile semi-transparent quad-port multi and wide-band antenna for 4G/5G/WLAN/Wi-Fi 6E applications,” *Optical and Quantum Electronics*, Vol. 55, No. 6, 552, 2023.
- [6] Aminu-Baba, M., M. K. A. Rahim, F. Zubir, A. Y. Iliyasa, K. I. Jahun, M. F. M. Yusoff, M. M. Gajibo, A. A. Pramudita, and I. K. C. Lin, “A compact triband miniaturized MIMO antenna for WLAN applications,” *AEU — International Journal of Electronics and Communications*, Vol. 136, 153767, 2021.
- [7] Cao, X., Y. Xia, L. Wu, H. Zhang, and Q. Zeng, “Two-port ring shaped MIMO antenna with quad-band,” *International Journal of RF and Microwave Computer-Aided Engineering*, Vol. 31, No. 9, e22782, 2021.
- [8] Ghosh, S., G. S. Baghel, and M. V. Swati, “A dual-port, single-fed, integrated microwave and mm-wave MIMO antenna system with parasitic decoupling mechanism for 5G-enabled IoT applications,” *AEU — International Journal of Electronics and Communications*, Vol. 176, 155122, 2024.
- [9] Karmokar, D. K. and S.-L. Chen, “Slot antenna miniaturization by loading dumbbell-shaped slots and strips, square-shaped loops, and shorting vias,” *Microwave and Optical Technology Letters*, Vol. 62, No. 6, 2307–2310, 2020.
- [10] Luo, M., X. Sang, J. Tan, and J. Chen, “A novel miniaturized metamaterial lens antenna,” *International Journal of RF and Microwave Computer-Aided Engineering*, Vol. 30, No. 7, e22219, 2020.

- [11] Dao, D. N. and J.-Y. Chung, "A miniaturized thin-film UWB monopole antenna implemented with high-DK adhesive," *Electronics*, Vol. 12, No. 16, 3445, 2023.
- [12] Shao, Z. and Y. Zhang, "A single-layer miniaturized patch antenna based on coupled microstrips," *IEEE Antennas and Wireless Propagation Letters*, Vol. 20, No. 5, 823–827, 2021.
- [13] Khan, A. A., S. A. Naqvi, M. S. Khan, and B. Ijaz, "Quad port miniaturized MIMO antenna for UWB 11 GHz and 13 GHz frequency bands," *AEU — International Journal of Electronics and Communications*, Vol. 131, 153618, 2021.
- [14] Chen, D., Q. Xue, W. Yang, K.-S. Chin, H. Jin, and W. Che, "A compact wideband low-profile metasurface antenna loaded with patch-via-wall structure," *IEEE Antennas and Wireless Propagation Letters*, Vol. 22, No. 1, 179–183, 2023.
- [15] Qin, Y., R. Li, and Y. Cui, "Embeddable structure for reducing mutual coupling in massive MIMO antennas," *IEEE Access*, Vol. 8, 195 102–195 112, 2020.
- [16] Ma, R., H. Huang, X. Li, and X. Wang, "Triple-band MIMO antenna with integrated decoupling technology," *International Journal of Antennas and Propagation*, Vol. 2023, No. 1, 6691346, 2023.
- [17] Ameen, M. and R. K. Chaudhary, "Isolation enhancement of metamaterial-inspired two-port MIMO antenna using hybrid techniques," *IEEE Transactions on Circuits and Systems II: Express Briefs*, Vol. 70, No. 6, 1966–1970, 2023.
- [18] Sharma, N. and S. S. Bhatia, "Metamaterial inspired fidget spinner-shaped antenna based on parasitic split ring resonator for multi-standard wireless applications," *Journal of Electromagnetic Waves and Applications*, Vol. 34, No. 10, 1471–1490, 2020.
- [19] Yang, R., S. Xi, Q. Cai, Z. Chen, X. Wang, and G. Liu, "A compact planar dual-band multiple-input and multiple-output antenna with high isolation for 5G and 4G applications," *Micromachines*, Vol. 12, No. 5, 544, 2021.
- [20] Kansal, P., A. K. Mandpura, and N. Kumar, "A dual band CPW-fed MIMO antenna for fifth generation application," *Physica Scripta*, Vol. 99, No. 5, 055548, 2024.
- [21] Verulkar, S. M., A. Khade, M. A. Trimukhe, and R. K. Gupta, "Compact wideband four elements MIMO antenna for 5G applications," *Progress In Electromagnetics Research C*, Vol. 137, 199–209, 2023.
- [22] Wu, D., Y. Qiu, G. Yu, R. Guo, G. Wu, J. Wang, Y. Zhang, M. Zhu, and H.-M. Zhou, "Decoupling technique using ferrite-film loading for 5G MIMO applications," *International Journal of Antennas and Propagation*, Vol. 2022, No. 1, 2028146, 2022.
- [23] Dou, Y., Z. Chen, J. Bai, Q. Cai, and G. Liu, "Two-port CPW-fed dual-band MIMO antenna for IEEE 802.11 a/b/g applications," *International Journal of Antennas and Propagation*, Vol. 2021, No. 1, 5572887, 2021.
- [24] Naidu, P. V., M. B. Dhanekula, K. M. Almustafa, A. Kumar, K. A. Meerja, and S. H. Akkapanthula, "Design and performance analysis of MAZE shaped quad port ACS fed tri band MIMO antenna for V2V and multi band applications," *AEU — International Journal of Electronics and Communications*, Vol. 134, 153676, 2021.
- [25] Usha Devi, Y., M. T. P. Boddapati, T. A. Kumar, K. Skc, and P. Pardhasaradhi, "Conformal printed MIMO antenna with DGS for millimeter wavecommunication applications," *International Journal of Electronics Letters*, Vol. 8, No. 3, 329–343, 2020.
- [26] Babu, B. A., B. T. P. Madhav, K. Srilatha, B. M. S. Sriram, and A. V. Hemanth, "A compact dual-band self-diplexing MIMO patch antenna for ism and X-band communications," *Journal of Microwaves, Optoelectronics and Electromagnetic Applications*, Vol. 21, No. 2, 319–327, 2022.